Aluminum Distribution in High-silica Mordenite

Baowang Lu[1,2], Takahide Kanai[1], Yasunori Oumi[1] and Tsuneji Sano[1,3]*

(1) School of Materials Science, Japan Advanced Institute of Science and Technology, Nomi, Ishikawa 923-1292, Japan

(2) Present address: Molecular Catalysis Group, Research Institute for Innovation in Sustainable Chemistry, National Institute of Advanced Industrial Science and Technology, Tsukuba, Ibaraki 305-8565, Japan

(3) Present address: Department of Applied Chemistry, Graduate School of Engineering, Hiroshima University, Higashi-Hiroshima 739-8527, Japan, E-mail: tsano@hiroshima-u.ac.jp

Abstract

The Al distribution in high-silica MOR zeolites with various Si/Al ratios was investigated by FT-IR spectroscopy in the presence of CD_3CN probe molecules and benzene adsorption. Two adsorption bands assigned to CN stretching vibration were observed at 2280-2295 and ≈ 2315 cm^{-1}, which are due to interaction of CN with acidic

hydroxyl groups in the main channels and the side pockets of H-MOR zeolite, respectively. The relative intensity of the peak at 2315 cm^{-1} increased with an increase in the Si/Al ratio, indicating that the proportion of Al atoms in the main channels relatively decreased with the Si/Al ratio. This was confirmed from the linear relationship between the number of benzene molecules adsorbed in a unit cell and the number of Al atoms in the main channels. In addition, this was also suggested from the computer simulation result that Al atoms are preferentially sitting in the T_3 site.

Keywords Mordenite, Main channel, Side pocket, Al distribution, Acetonitrile

1 Introduction

Mordenite (MOR) zeolite is a high-silica zeolite with an ideal composition of $Na_8[Al_8Si_{40}O_{96}]\cdot 24H_2O$ [1]. The hydrothermal synthesis of MOR zeolite was first reported by Barrer et al. [2,3] and then many researchers have reported several synthesis methods for high-silica MOR zeolites with Si/Al ratios of 7.5-15 [4-6]. Due to its high thermal and acid stabilities, MOR zeolite is one of industrially important zeolites and widely used for many processes in petroleum refining and petrochemical industries such as hydrocracking, hydroisomerization, alkylation and dimethylamines synthesis [7-9].

Recently, MOR zeolite has also been proposed to apply for hosts of semiconductor materials, chemical sensors and nonlinear optical materials [10].

It is well known that MOR zeolite has a pore system consisting of a parallel linear channels with main channel composed of 12- membered ring (MR) (6.5×7.0 Å) running along to the *c*-axis and another one called side pocket composed of 8-MR (2.6×5.7 Å) running along to the *b*-axis (Fig. 1). Bodart et al. reported that Al atoms preferentially occupy tetrahedral positions in the four-membered ring of the MOR zeolite structure, T_3 and T_4 sites [11]. The T_3 sites are located in the bottom of the side pockets, whereas the T_4 sites are faced on the 12-MR main channels. These strongly suggest an existence of two different hydroxyl groups with different acid strength, which probably reflects slight difference in the local environment. Therefore, many researchers have investigated the Al distribution in the MOR zeolite structure using crystalgraphical and spectroscopic data [12-21]. From the adsorption-desorption experiments of probe molecules such as CO, pyridine and CD_3CN monitored by FT-IR spectroscopy, it was found that two types of Brønsted acid sites exist in H-MOR zeolite. One is attributed to the acidic OH group of Si(OH)Al in the main channels (HF (high frequency band) at 3612 cm^{-1}); and the other is associated with the acidic OH group in the site pockets (LF (low frequency band) at 3585 cm^{-1}). In literature reported so far, the HF/LF intensity ratio, the Al distribution, have been considered to be independent of the Si/Al ratio of H-MOR zeolite because of no experiments using H-MOR zeolites with the higher Si/Al

ratios of more than 10.

We have studied the direct hydrothermal synthesis of high-silica MOR zeolite by various methods. Very recently, the highly crystalline MOR zeolite with a bulk Si/Al ratio of ≈ 30 was successfully prepared using both tetraethylammonium hydroxide as a structure-directing agent and NaF as a fluoride source, when $Al(NO_3)_3$ was employed as an aluminum source [22,23]. The addition of seed crystals or NH_4NO_3 as a mineralizer was also found to be very effective for direct synthesis of high-silica MOR zeolite [24,25]. However, characteristics of the as-synthesized MOR zeolites such as textural property and Al distribution were not clarified.

From such viewpoints, we investigated the correlation between the content and the distribution of Al atoms in MOR zeolite using the prepared high-silica MOR zeolites in this paper.

2 Experimental

2.1 Synthesis of high-silica MOR zeolite using various additives

The hydrothermal synthesis of MOR zeolite was carried out using different additives such as seed crystals or NaF. The starting mixtures were prepared as follows.

$Al(NO_3)_3 \bullet 9H_2O$ (Wako Pure Chemical, Japan, 98.0 %) was mixed with an aqueous solution containing NaOH (Merck-Schuchardt, Germany, 99 %) and tetraethylammonium hydroxide (TEAOH, Aldrich, USA, 35 wt%). Then the precipitated hydrated silica (Nipsil, Nippon Silica Ind., Japan, SiO_2 = 88 wt%, H_2O = 12 wt%) was added to the mixture and was homogenized in a mortar. Finally, 4 wt% of seed crystals based on the weight of the precipitated silica or NaF as a fluoride source (Wako Pure Chemical, Japan, 99.0 %) was added, and homogenization was continued until a uniform gel was obtained. The chemical composition of the starting synthesis gel prepared was as follows: Si/Al = 15−30, H_2O/SiO_2 = 7.4 or 15, NaOH/Al = 3−6, $TEAOH/SiO_2$ = 0 or 0.23, NaF/SiO_2 = 0 or 0.8. The gel thus obtained was charged into a 30 cm^3 stainless steel autoclave equipped with a Teflon liner and kept at 170 °C for 3 days under static conditions. The solid product was filtered, washed thoroughly with 1,000 cm^3 of deionized hot water (60 °C), dried overnight in oven at 120 °C and calcined at 500 °C for 10 h. NH_4^+ and Na^+ ion-exchange of MOR zeolites were carried out using 1 M NH_4NO_3 and NaCl aqueous solutions at 80 °C for 2 h under stirring conditions, respectively, and the ion-exchange treatment was repeated three times.

2.2 Characterization

The X-ray diffraction (XRD) patterns of the solid products were collected by a

powder X-ray diffractometer (Rigaku, RINT 2000) with graphite monochromatized Cu Kα radiation at 40 kV and 30 mA. The bulk chemical compositions were measured by X-ray fluorescence (XRF, Philips Spectrometer PW 2400). The crystal morphology of MOR zeolite was measured by scanning electron microscopy (SEM, Hitachi S-4000) operated at 20 kV after sputter-coating with platinum. Nitrogen adsorption isotherms at –196 °C were measured using a conventional volumetric apparatus (Bel Japan BELSORP 28SA). Prior to adsorption measurements, the powder zeolites (≈ 0.1 g) were evacuated at 400 °C for 10 h. ^{27}Al MAS NMR spectra of MOR zeolites were recorded using a zirconia rotor with 7 mm diameter on a Varian VXP-400 at 104.2 MHz. $Al(NO_3)_3 \bullet 9H_2O$ was used as a chemical shift reference. Prior to the ^{27}Al MAS NMR measurements, the sample was moisture-equilibrated over a saturated solution of NH_4Cl for 24 h.

The FT-IR spectra of adsorbed CD_3CN were measured on a FT-IR spectrometer (JEOL JIR-7000) with a resolution 4 cm^{-1}at room temperature. The sample (NH_4-MOR) was pressed into a self-supporting thin wafer and placed in a quartz IR cell with CaF_2 windows. The protonic form (H-MOR) was obtained by thermal treatment of the NH_4-MOR zeolite in the IR cell under vacuum (10^{-3} torr) at 450 °C for 2 h. The adsorption of acetonitrile-d3 (CD_3CN, Aldrich, 99.9%) on the H-MOR zeolite was carried out at 100 °C for 1 h, and then evacuated at 150 °C for 1 h to remove excess and weakly adsorbed CD_3CN.

Benzene adsorption of Na-MOR zeolite was measured using a conventional volumetric apparatus (Bel Japan BELSORP 18A) at 25 °C. Prior to adsorption measurements, the powder zeolites (≈ 0.2 g) were evacuated at 400 °C for 10 h.

2.3 Computer simulation

DFT (Density functional theory) quantum chemical calculation was performed using the DMol3 package in Materials Studio (version 3.2) developed by Accelrys, Inc. on Appro HyperBlade Cluster integrated by Best Systems, Inc. [26,27]. The geometry optimization calculation was carried out using double numerical polarization basis set with polarization functions (DNP), whose size is comparable to Gaussian 6-31G^{++}. The nonlocal gradient corrected potential (Perdew-Burke-Evnzenhof (PBE)) was employed for geometry optimization and evaluation of the total energy of the final optimized geometry [28,29].

Cluster model: There are four symmetrically independent tetrahedral sites (labeled T_1-T_4) in the unit cell of MOR zeolite structure, as shown in Fig. 1. This lead to four possible positions for framework Al atoms: T_1 and T_2 in the 6-MR sheets, T_3 and T_4 located in the 4-MR. The initial geometry of the cluster model for quantum chemical calculation is derived from the crystal structure reported by X-ray diffraction study. The stoichiometry of the cluster models of T_1 and T_2 sites is $H_{13}AlSi_4O_{16}$, whereas T_3 and T_4

sites $H_{13}AlSi_5O_{18}$. Adjacent silicon atoms bonded to oxygen atoms were replaced by hydrogen atoms. This technique is obviously not perfect but frequently is used as methodology of saturating dangling bonds on cluster boundaries. Selecting the proper cluster for zeolitic structure is itself a subject of many studies. As our interest is the local structure around the incorporated metal center, our choice seems to be rather a modest one. We believe that this cluster is adequate to reproduce basic features of a local electronic structure of an active center in the zeolitic framework. On the other hand, it offers the possibility of employing the highest level of computational accuracy required for the evaluation of electronic properties.

The stabilization energies were calculated by subtracting the energies of gas-phase atoms and the siliceous cluster model from the energy of the optimized system. For example, the stabilization energy of aluminum substituted cluster was calculated as follows:

Est = {E(aluminum substituted cluster) + E(silicon atom)}

– {E(siliceous cluster) + E(aluminum atom) + E(hydrogen atom)}

In here, Est: stabilization energy, E(aluminum substituted cluster): total Energy for optimized $H_{13}AlSi_4O_{16}$ (T_1 and T_2 site model) and $H_{13}AlSi_5O_{18}$ (T_3 and T_4 site model) cluster, E(silicon atom): total energy for a Si atom, E(siliceous cluster): total energy for $H_{12}Si_5O_{16}$ (T_1 and T_2 site model) and $H_{12}Si_6O_{18}$ (T_3 and T_4 site model), E(aluminum atom): total energy for a Al atom, E(hydrogen atom): total energy for a H atom. With

this definition, a negative Est corresponds to the stable substitution of aluminum in the MOR zeolite framework.

3 Results and Discussion

3.1 Synthesis of high-silica MOR zeolite

The synthesis results of MOR zeolites obtained from starting gels having various chemical compositions with different additives are summarized in Table 1 together with the synthesis conditions. Fig. 2 shows the XRD patterns of the as-synthesized MOR zeolites. All of the prepared MOR zeolites were highly crystalline and no other peaks other than those corresponding to MOR zeolite were observed. The Si/Al ratios of the prepared MOR zeolites were 8.4-26.5.

The typical SEM images of various MOR zeolites obtained are shown in Fig. 3. In the case of MOR zeolite synthesized without TEAOH (Sample no.1), the morphology of MOR zeolite crystals was not regular and the average crystal length was ≈ 20 μm. On the other hand, when TEAOH was employed as a structure-directing agent, the rectangular parallelepiped and rice-grain-like crystals were obtained and the average crystal length was ≈ 15 μm regardless NaF addition (Sample nos. 2 and 3). In the case

of MOR zeolites prepared using seed crystals, the rectangular parallelepiped crystals with the crystal length of ≈ 5 μm (Sample no. 4) and the leaf-like crystals (Sample no. 5) with the crystal length of ≈ 7.5 μm were obtained from the starting gels with Si/Al ratios of 20 and 30, respectively.

The ^{27}Al MAS NMR spectra of these MOR zeolites are shown in Fig. 4. Only a sharp signal at ≈ 54 ppm was observed, which is a characteristic resonance of tetrahedrally coordinated framework aluminum species. No signal assigned to non-framework aluminum species was observed around 0 ppm. Therefore, it was clearly revealed that all aluminums present in the MOR zeolites are present in the zeolitic framework.

To obtain a qualitative assessment of microporosity of the obtained high-silica MOR zeolites, nitrogen adsorption isotherms were measured. As listed in Table 1, there were almost no differences in the BET surface area and the micropore volume determined by the t-plot method. These values are similar to those of commercially available MOR zeolite.

3.2 Al distribution in high-silica MOR zeolite

As acetonitrile is a base molecule and is small enough to penetrate the side pockets of MOR zeolite, it can react easily with the acidic hydroxyl groups (Si(OH)Al) located in the side pockets. Therefore, it is possible to distinguish the localization of the two

different hydroxyl groups present in the main channels and the side pockets of MOR zeolite, namely the Al distribution. Fig. 5 shows the IR spectra of CD_3CN adsorbed on the H-MOR zeolites in the ν (CN) vibration region. For all samples, the band assigned to CN stretching vibration of CD_3CN interacting with the acidic OH groups in the side pockets of MOR zeolites was observed at ≈ 2315 cm^{-1} [19]. On the other hand, the band assigned to CN stretching vibration of CD_3CN interacting with the acidic OH groups in the main channels of MOR zeolites appeared at 2280-2295 cm^{-1} [19], which was slightly dependent upon the Si/Al ratio. The exact reason for the Si/Al ratio dependence of the frequency shift was not clarified at the present time. The intensity ratio ($I_{2315\ cm\text{-}1}/I_{2280\text{-}2295\ cm\text{-}1}$) for the H-MOR zeolite with a Si/Al ratio of 8.4 (Sample no. 1) was about 0.43. This value was roughly consistent with the value reported in literature, which was calculated from the intensity ratio of two bands at 3612 and 3585 cm^{-1} in the FT-IR spectra of H-MOR zeolite. It is generally agreed that the 3612 and 3585 cm^{-1} bands are assigned to acidic hydroxyls located in the main channels and in the side pockets, respectively [12,15]. These results strongly indicate that the Al distribution of MOR zeolite is strongly affected by the Si/Al ratio. In Fig. 6, the intensity ratio ($I_{2315\ cm\text{-}1}/I_{2280\text{-}2295\ cm\text{-}1}$) is plotted against the number of Al atoms in a unit cell (u.c.) of MOR zeolite. It was found that the intensity ratio decreases linearly with an increase in the number of Al atoms, indicating the higher proportion of Al atoms in the side pockets of high-silica MOR zeolites.

To investigate the further information about the Al distribution of high-silica MOR zeolites, the benzene adsorption experiments were also carried out on Na-MOR zeolites. The benzene adsorption isotherms of Na-MOR zeolites with the Si/Al ratios of 8.4 and 19.1 are shown in Fig. 7. Although both isothems exhibited type I behavior, a slight difference in the amount of benzene adsorbed was observed. The increase in the amount of benzene adsorbed by the multilayer adsorption of benzene molecules on the external surfaces of zeolite crystals was only observed at the P/P_0 of more than 0.95 for Sample no. 4, suggesting a small contribution of benzene adsorption on the external surfaces. Therefore, the adsorption capacity of benzene was determined by the Langmuir plot. Fig. 8 shows the relationship between the number of benzene molecules adsorbed in a unit cell and the number of Al atoms in the main channels in a unit cell. The number of Al atoms in the main channels was calculated by using the intensity ratio $I_{2315\ cm\text{-}1}/I_{2280\text{-}2295\ cm\text{-}1}$ given in Fig. 6. Of course, it is assumed that the intensity ratio reflects the proportion of Al atoms located in the main channels and the side pockets of MOR zeolite. The good linear relationship was observed, suggesting that benzene adsorption is strongly affected by the number of Al atoms in the main channels. Although Itabashi et al. have already reported the similar results, however, the MOR zeolites with high Al content, the Si/Al ratio of 5-12, were employed [30, 31]. Taking into account that benzene molecules can not enter into the side pockets due to its molecular size, this strongly indicates that Na^+ cations present in the main channels hinder diffusion of

benzene molecules into the channels and exclude benzene molecules. When the line is extrapolated to 0 of the number of Al atoms, the number of adsorbed benzene molecules is ≈ 3.7 in a unit cell, which is consistent with the value reported in the literature [20, 28].

Next, to get information concerning an influence of NaF addition in the starting synthesis gel on the Al distribution of high-silica MOR zeolite, the CD_3CN adsorption was carried out on the high-silica MOR zeolites synthesized with and without NaF. Fig. 9 shows the FT-IR spectra of CD_3CN adsorbed on the H-MOR zeolites synthesized with and without NaF (Sample nos. 2 and 3). There is no difference in the spectra between these two high-silica MOR zeolites. Although Kato et al. have recently concluded that there is a different distribution of Al atoms in the framework between MOR zeolites with a low Si/Al ratio synthesized with and without NaF in the absence of TEAOH [20], these results strongly indicate that there is no difference in the Al distribution in the MOR zeolites with a high Si/Al ratio synthesized in the presence of TEAOH. Although we could not explain the reason at the present time due to a limited data, probably it is due to the higher alkalinity of the synthesis gel as compared with the conventional synthesis method without TEAOH.

3.3 Computer simulation

Stabilization energies of various cluster models were calculated through generalized gradient approximation (GGA), in which each T (T_1~T_4) site was replaced by Al atom. Although no big difference was observed among these models, the stabilization energy calculated decreased in the following order: $T_3 > T_4 > T_1 > T_2$, as shown in Fig. 10. Namely, T_3 is the most stable site among these four sites. Therefore, Al atom is preferentially sitting in the T_3 site of MOR zeolite. This result strongly supports those obtained by CD_3CN and benzene adsorption experiments.

4 Conclusions

Highly crystalline and pure high-silica MOR zeolites with different Si/Al ratios from 8.4 to 26.5 were prepared, and an influence of the Si/Al ratio on the Al distribution of MOR zeolites was investigated. It was found from CD_3CN and benzene adsorption experiments that the Al distributions in high-silica MOR zeolites with Si/Al ratios of more than 10 are strongly dependent upon the Si/Al ratio. The proportion of Al atoms in the main channels relatively decreased with an increase in the Si/Al ratio of MOR zeolite. This was also supported by the simulation result.

Acknowledgment

The authors wish to acknowledge Dr. Keiji Itabashi at Nanyo Research Laboratory, Tosoh Corporation for useful discussion and advice.

References

(1) D.W. Breck, Zeolite Molecular Sieves: Structure, Chemistry and Uses, Wiley, New York, 1974.

(2) R.M. Barrer, J. Chem. Soc., 127 (1948).

(3) R.M. Barrer and E.A.D. White, J. Chem. Soc., 1261 (1951).

(4) O.J. Whittemore JR., Amer. Mineralogist, 57, 1146 (1972).

(5) S. Sakurada, N. Tagaya, T. Maeshima, T. Toyoizumi, T. Numura and T. Hasimoto, Euro Pat. 0040104 (1981).

(6) J. Arika, H. Miyazaki, K. Itabashi and M. Aimoto, Euro Pat. 0109729 (1984).

(7) P.K. Bajpai, Zeolites 6, 2 (1986).

(8) I.E. Maxwell and W.H.J. Stork, edited by H. von Bekkum, E.M. Flanigen and J.C. Jonsen, Introduction to Zeolite Science and Practice, Elsevier, Amsterdam, 1991, p.71.

(9) L.D. Fernandes, J.L.F. Monteiro, E.F. Sousa-Aguiar, A. Martinez and A. Corma, J.

Catal. 177, 363 (1998).

(10) J.E. Gilbert and A. Mosset, Mater. Res. Bull. 33, 997 (1998).

(11) P. Bodart, J.B. Nagy, G. Debras, Z. Gabelica and P.A. Jacobs, J. Phys. Chem. 90, 5183 (1986).

(12) F. Wakabayashi, J. Kondo, A. Wada, K. Domen and C. Hirose, J. Phys. Chem. 97, 10761 (1993).

(13) V.L. Zholobenko, M.A. Makarova and J. Dwyer, J. Phys. Chem. 97, 5962 (1993).

(14) M. Maache, A. Janin, J.C. Lavalley and E. Benazzi, Zeolites 15, 507 (1995).

(15) S. Bordiga, C. Lamberti, F. Geobaldo and A. Zecchina, Langmuir 11, 527 (1995).

(16) J. Datka, B. Gill and A. Kubacka, Zeolites 17, 428 (1996).

(17) A. Alberti, Zeolites 19, 411 (1997).

(18) R. Anquetil, J. Saussey and J.C. Lavalley, Phys. Chem. Chem. Phys. 1, 555 (1999).

(19) O. Marie, F. Thibault-Starzyk and J.C. Lavalley, Phys. Chem. Chem. Phys. 2, 5341 (2000).

(20) M. Kato, K. Itabashi, A. Matsumoto and K. Tsutumi, J. Phys. Chem. B 107, 1788 (2003).

(21) O. Marie and F. Thibault-Starzyk, J. Phys. Chem. B 108, 5073 (2004).

(22) H. Sasaki, Y. Oumi, K. Itabashi, B.-W. Lu, T. Teranishi and T. Sano, J. Mater. Chem. 13, 1173 (2003).

(23) B.-W. Lu, T. Tsuda, H. Sasaki, Y. Oumi, K. Itabashi, T. Teranishi and T. Sano,

Chem. Mater. 16, 286 (2004).

(24) B.-W. Lu, T. Tsuda, Y. Oumi, K. Itabashi and T. Sano, Micropor. Mesopor. Mater. 76, 1 (2004).

(25) B.-W. Lu, Y. Oumi, K. Itabashi and T. Sano, Micropor. Mesopor. Mater. 81, 365 (2005).

(26) B. Delley, J. Chem. Phys. 92, 508 (1990).

(27) B. Delley, J. Chem. Phys. 113, 7756 (2000).

(28) J. P. Perdew, K. Burke, and M. Ernzerhof, Phys. Rev. Lett. 77, 3865 (1996).

(29) J. P. Perdew, K. Burke, and M. Ernzerhof, Phys. Rev. Lett . 78, 1396 (1997).

(30) K. Itabashi, T. Fukushima and K. Igawa, Zeolites 6, 30 (1986).

(31) K. Itabashi, T. Okada and K. Igawa, edited by Y. Murakami, A. Iijma and J.W. Ward, Proceeding of the 7th International Zeolite Conference, Kodansha, Tokyo, Japan, 1986, p. 369.

Table 1
Synthesis and characterization of high-silica MOR zeolites using various additives[a]

Sample no.	Synthesis starting gel						MOR zeolite			
	Si /Al	H_2O /SiO_2	NaOH /Al	NaF /SiO_2	TEAOH /SiO_2	Seeding	Si/Al ratio	Al/u.c.	BET surface area (m^2/g)	Number of benzene adsorbed (molecules/u.c.)
1	10	15	6	0	0	No	8.4	5.11	456	3.06
2	15	7.4	3	0	0.23	No	15.9	2.84	451	3.36
3	15	7.4	3	0.8	0.23	No	15.6	2.89	484	3.64
4	20	7.4	4	0	0.23	Yes	19.1	2.39	491	3.48
5	30	7.4	6	0	0.23	Yes	26.5	1.75	471	3.51

[a]Synthesis conditions: Seed crystals (4 wt%) = Sample no. 2, Temp. = 170 °C, Time = 3 days.

Figure captions

Fig. 1 MOR framework viewed along the c-axis. T_1-T_4 implies the four possible different sites of Al atoms.

Fig. 2. XRD patterns of various high-silica MOR zeolites.

Sample nos.: (a) 1, (b) 2, (c) 3, (d) 4, (e) 5.

Fig. 3. SEM images of various high-silica MOR zeolites.

Sample nos.: (a) 1, (b) 2, (c) 3, (d) 4, (e) 5.

Fig. 4. ^{27}Al MAS NMR spectra of various high-silica MOR zeolites.

Sample nos.: (a) 1, (b) 2, (c) 3, (d) 4, (e) 5.

Fig. 5 FT-IR spectra of CD_3CN adsorbed on H-MOR zeolites with various Si/Al ratios.

Sample nos.: (a) 1, (b) 2, (c) 4, (d) 5.

Fig. 6 Relationship between the number of Al atoms and the intensity ratio $I_{2315\ cm-1}/I_{2280-2295\ cm-1}$.

Fig. 7 Benzene adsorption isotherms of Na-MOR zeolites.

Sample nos.: (a) 1, (b) 4.

Fig. 8 Relationship between the number Al atoms in the main channels and the number of benzene molecules adsorbed.

Fig. 9 FT-IR spectra of CD_3CN adsorbed on H-MOR zeolites synthesized with and without NaF.

Sample no.: (a) 2, (b) 3.

Fig. 10 Calculated stabilization energies of various cluster models.

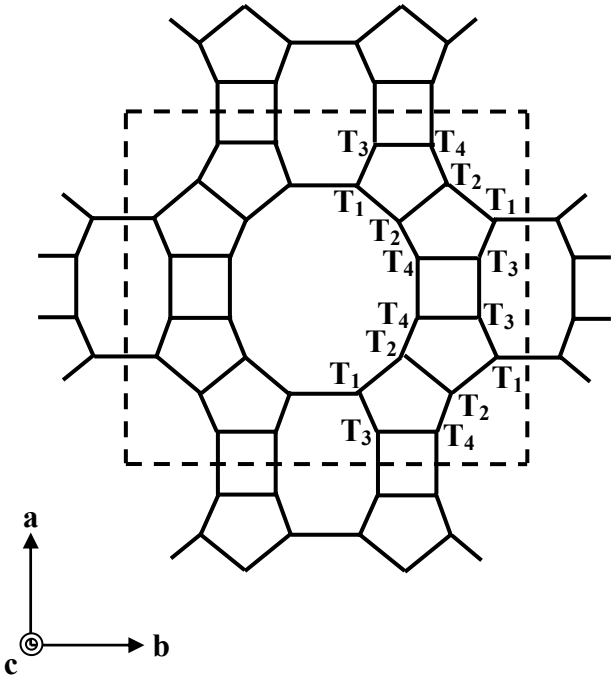

Figure 1.

Lu et al.

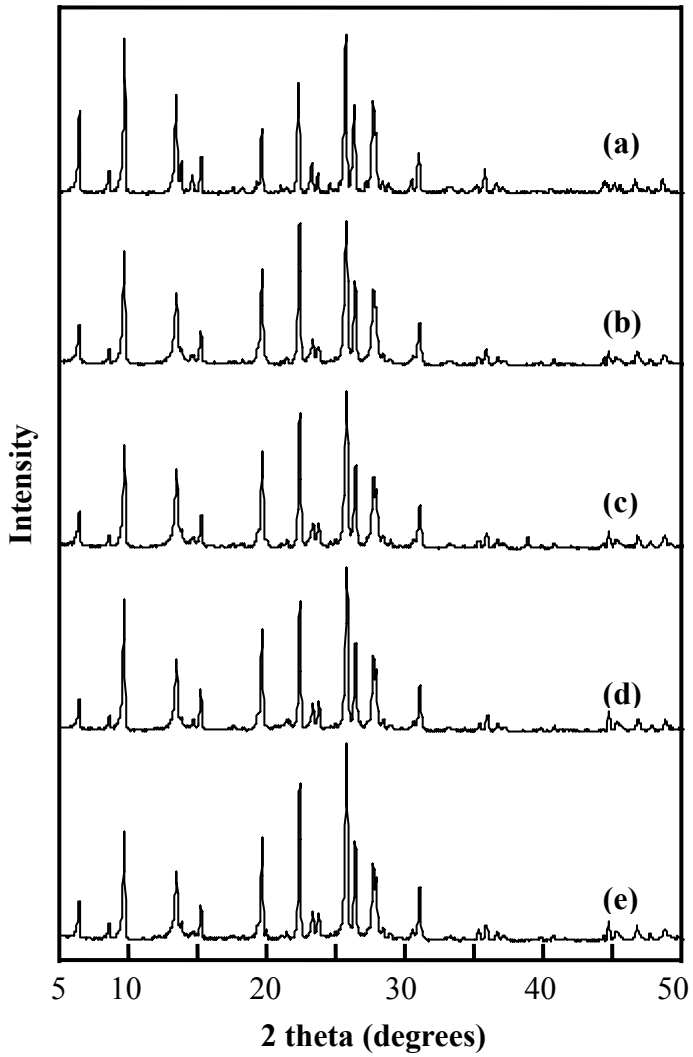

Figure 2.

Lu et al.

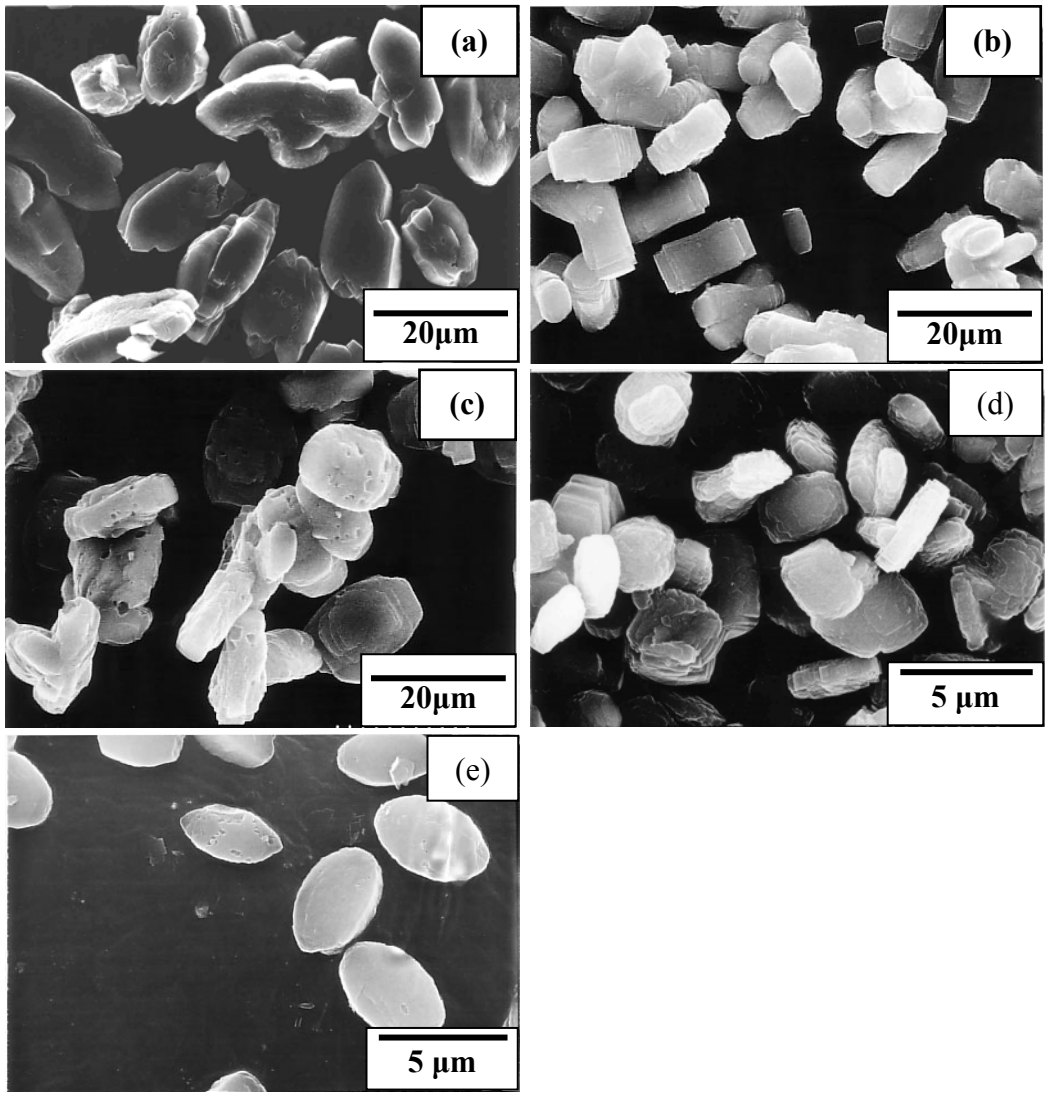

Figure 3.

Lu et al.

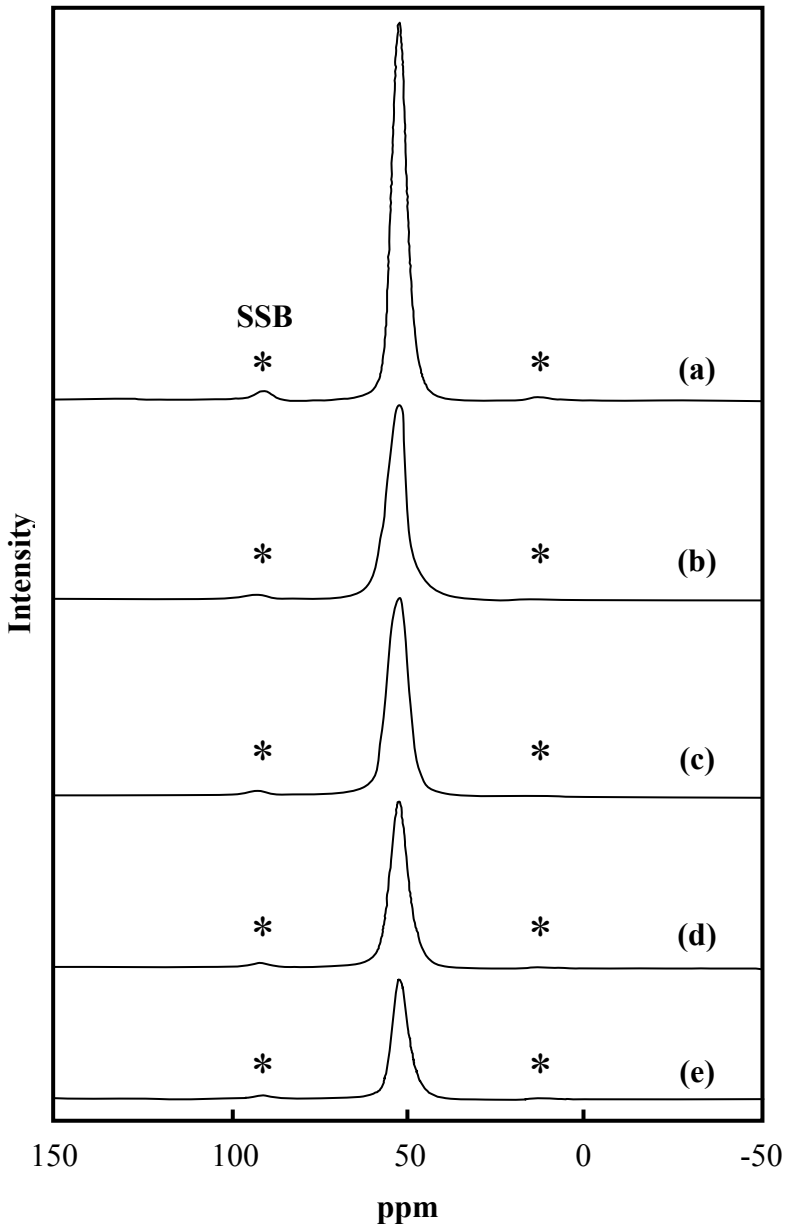

Figure 4.

Lu et al.

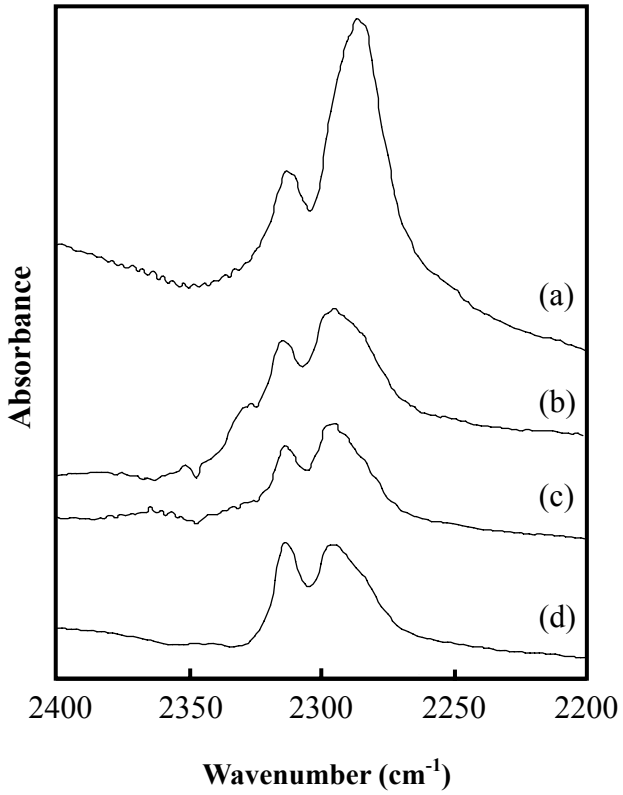

Figure 5.

Lu et al.

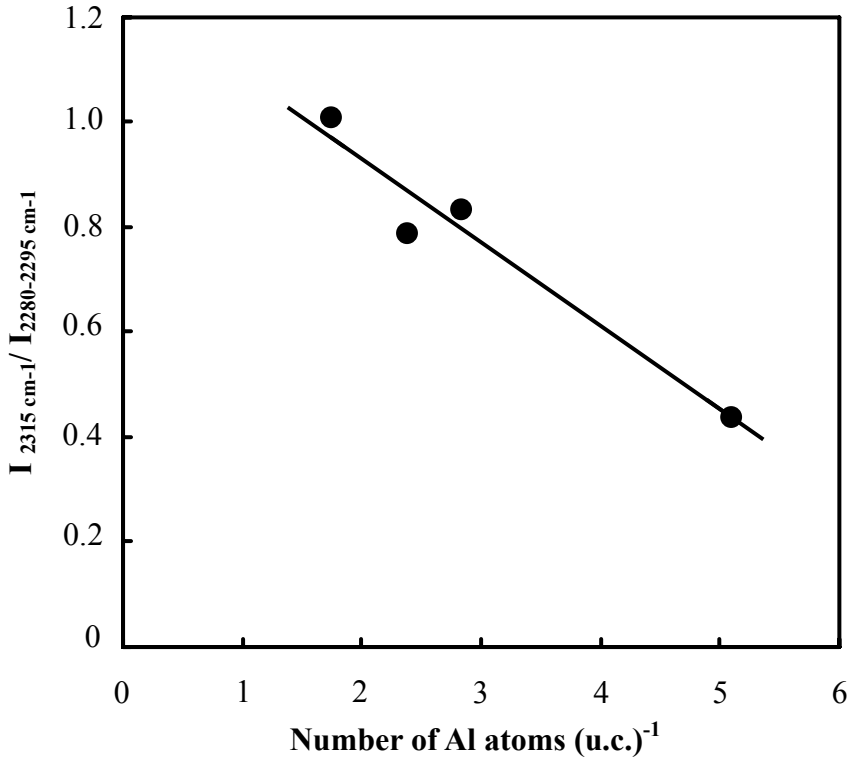

Figure 6.

Lu et al.

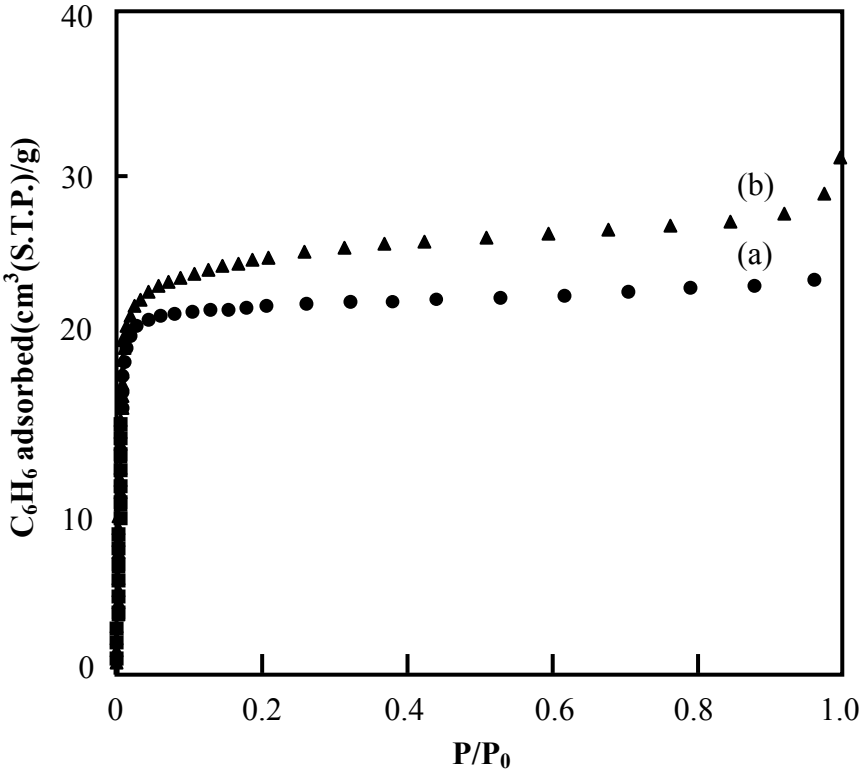

Figure 7.

Lu et al.

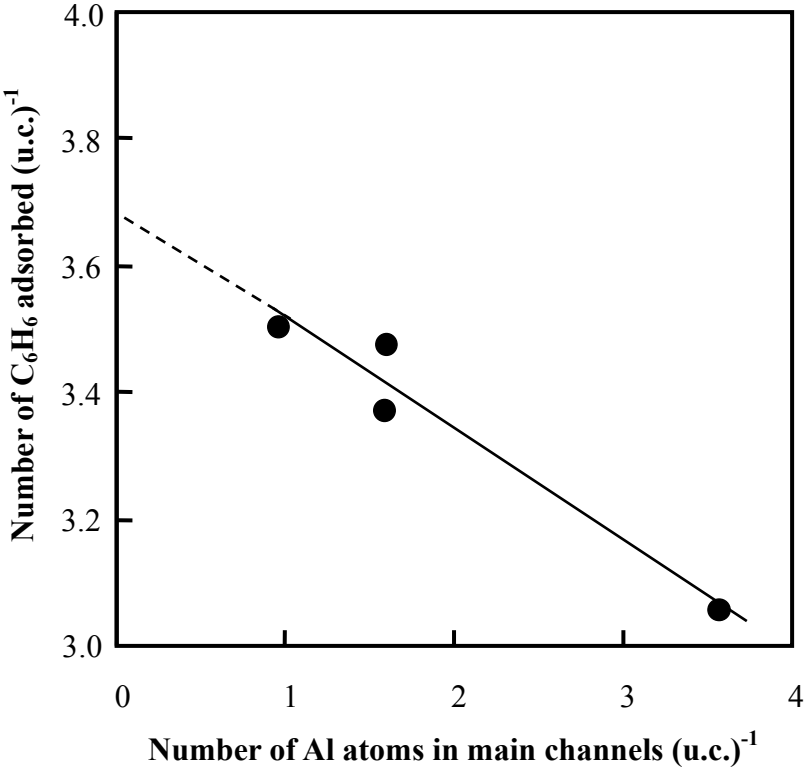

Figure 8.

Lu et al.

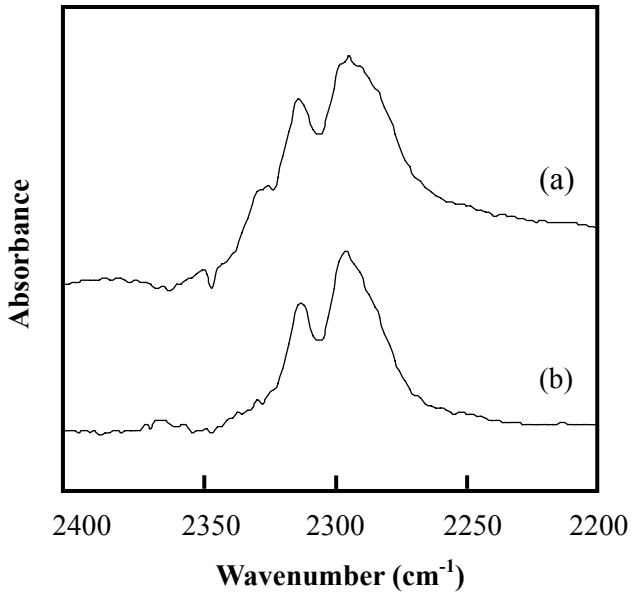

Figure 9.

Lu et al.

	T1 Main channel	T2 Main channel	T3 Side pocket	T4 Main channel
	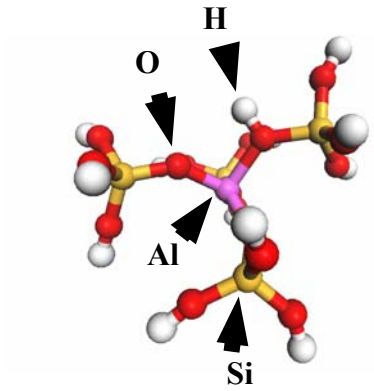	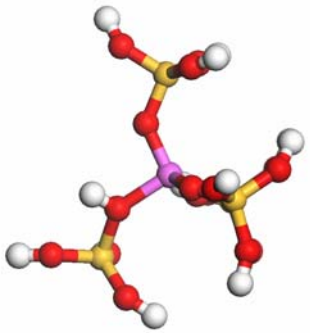	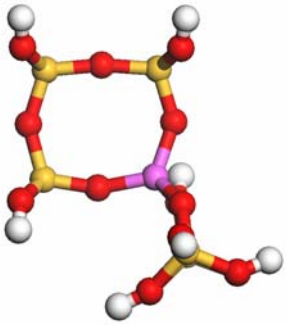	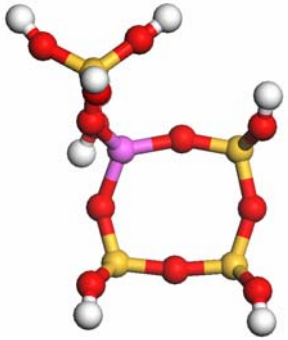
dE (kJ/mol)	- 113	- 105	- 134	- 127

Figure 10.

Lu et al.